

Virial Equation of State for a Granular System

by

Subhanker Howlader and Prasenjit Das¹

*Department of Physical Sciences, Indian Institute of Science Education and Research Mohali,
Knowledge City, Sector 81, SAS Nagar, Punjab 140306, INDIA*

Abstract

The equation of state for an ideal gas is simple, which is $P = nk_{\text{B}}T$. In the case of imperfect gases where mutual interactions among the constituents are important, pressure P can be expressed as the series expansion of density n with appropriate coefficients, known as virial coefficients B_m . In this paper, we have obtained the first four virial coefficients for a model interaction potential $\Phi(r)$ using multidimensional Monte-Carlo integration and importance sampling methods. Next, we perform molecular dynamics simulations with the same $\Phi(r)$ for a many-particle system to obtain P as a function of T and n . We compare our numerical data with the virial equation of state.

arXiv:2402.17100v2 [cond-mat.soft] 16 Mar 2024

¹prasenjit.das@iisermohali.ac.in

1. Introduction

Understanding the equilibrium properties of gases has been a centuries-old pursuit, tracing its origins from Boyle's (1662) to Charles's (1787) laws [1]. The combination of these with Gay-Lussac's and Avogadro's laws led to the synthesis of the ideal gas law: $PV = Nk_B T$ by Clapeyron in 1834. The Maxwell's speed distribution and finite size correction of *van der Waals* at high pressure improve our understanding further. For ideal gases, there is no mutual interaction among the gas particles. However, in reality, the behaviors of gases are more intricate due to mutual interactions among the particles. Therefore, we need to incorporate the contribution from the interaction potential $\Phi(r)$ into the equation of state (EoS). Historically, this has been done through the *cluster expansion* method by Mayer and his collaborators (1938–1951), known as *Mayer cluster expansion* [2]. They obtained the EoS as a series of the form [3]

$$\frac{P}{k_B T} = B_1(T)n + B_2(T)n^2 + B_3(T)n^3 + B_4(T)n^4 + \dots, \quad (1)$$

where $n(= N/V)$ is the density. The eq (1) is known as the virial equation of state, $B_m(T)$ is the temperature (T) dependent m^{th} virial coefficient, and k_B is the Boltzmann constant.

The virial coefficient $B_m(T)$ involves the interaction potential $\Phi(r)$ through the Mayer function $f_{ij} \equiv f(r_{ij}) = \exp\{-\beta\Phi(r_{ij})\} - 1$, where $\beta = (k_B T)^{-1}$ and r_{ij} is the distance between the centers of a pair of particles i and j . The mathematical expressions for the first four virial coefficients are as follows [2–4]:

$$B_1(T) = \frac{1}{V} \int d^3 r_1 = 1 \bullet \quad (2)$$

$$B_2(T) = -\frac{1}{2V} \iint f_{12} d^3 r_1 d^3 r_2 = -\frac{1}{2V} \bullet \text{---} \bullet \quad (3)$$

$$B_3(T) = -\frac{1}{3V} \iiint f_{12} f_{13} f_{23} d^3 r_1 d^3 r_2 d^3 r_3 = -\frac{1}{3V} \begin{array}{c} \bullet \\ / \quad \backslash \\ \bullet \text{---} \bullet \end{array} \quad (4)$$

$$B_4(T) = -\frac{1}{8V} \iiint\int [3f_{13}f_{14}f_{23}f_{24} + 6f_{12}f_{13}f_{14}f_{23}f_{24} + f_{12}f_{13}f_{14}f_{23}f_{24}f_{34}] d^3 r_1 d^3 r_2 d^3 r_3 d^3 r_4 \\ = -\frac{1}{8V} \left(3 \begin{array}{c} \bullet \quad \bullet \\ | \quad | \\ \bullet \quad \bullet \end{array} + 6 \begin{array}{c} \bullet \quad \bullet \\ / \quad \backslash \\ \bullet \quad \bullet \end{array} + \begin{array}{c} \bullet \quad \bullet \\ / \quad \backslash \\ \bullet \quad \bullet \end{array} \right) \quad (5)$$

In eqs (2) – (5), points represent particles, and lines are bonds between them such that they have an interaction. Each bond corresponds to a Mayer function in the integrals. If there are no bonds, then there are no interactions ($f_{ij} = 0$). Clearly, the calculation of $B_m(T)$ involves integration over a large number of m -particle irreducible graphs. The number of such graphs increases exponentially with m , making the calculation of higher-order $B_m(T)$ s cumbersome. By definition, $B_1(T) = 1$ and $B_m(T) = 0$ for $m > 1$ for ideal gases and nonzero for imperfect gases. Thus, $B_m(T)$ s act as a measure of deviation from the ideal gas behavior.

There exist theoretical and numerical evaluations of virial coefficients for many model systems [5]. For piece-wise constant potentials, e.g., hard-sphere, square-well, etc., an exact analytical calculation of $B_m(T)$ s is possible up to a certain order. For example, Boltzmann

analytically calculated $B_3(T)$ and $B_4(T)$ in spatial dimension $d = 3$ for hard spheres (HS) [6]. Later, Luban and Barum extended the calculation of $B_3(T)$ for an arbitrary d [7]. Clisby and McCoy calculated $B_4(T)$ in $d = 4, 6, 8, 10, 12$ [8], and Lyberg in $d = 5, 7, 9, 11$ [9] for the same system. For attractive square-well (SW) potential, Kihara analytically obtained $B_2(T)$ and $B_3(T)$ for arbitrary range of attraction λ [10]. Katsura calculated $B_4(T)$ for λ equals the molecular diameter [11]. Later, Barker and Monaghan observed some discrepancies in Katsura's work and proposed a more accurate method [12] to evaluate $B_4(T)$. The rest of the higher-order virial coefficients, i.e., $B_m(T)$ s for $m > 4$, are evaluated numerically. For example, Ree and Hoover calculated $B_5(T)$ to $B_7(T)$ [13,14], van Rensburg calculated $B_8(T)$ [15], Labik *et al.* calculated $B_9(T)$ [16], and Clisby and McCoy calculated $B_{10}(T)$ for HS systems for different spatial dimensions [17]. For SW potential, Do *et al.* calculated $B_5(T)$ to $B_9(T)$ numerically [18].

For continuous nonlinear potentials, e.g., Lennard-Jones (LJ), repulsive inverse power, etc., an exact calculation of virial coefficients is difficult. For LJ potential [$U_{LJ}(r) = (M/r^\alpha) - (N/r^\beta)$], Garrett obtained $B_2(T)$ in a closed form for $\alpha = 2\beta$ [19]. Later, Kihara calculated $B_3(T)$ for $N, M > 0$ and $\alpha > \beta > 3$ [10]. Using numerical methods, Barker *et al.* calculated up to B_5 for LJ systems in $d = 2$ and $d = 3$ [20,21]. Singh and Kofke calculated from $B_2(T)$ to $B_6(T)$ [22] using the umbrella sampling method for the standard LJ system. Later, Schultz and Kofke extended the study up to $B_8(T)$ [23], and recently, Feng *et al.* to $B_{16}(T)$ [24]. For repulsive inverse-power-law potential [$U_{LJ}(r)$ with $N = 0$], Kihara obtained $B_2(T)$ and $B_3(T)$ [10], and Dixon and Hutchinson calculated $B_4(T)$ for $\alpha \geq 4$ analytically [25]. Wheatley obtained from $B_3(T)$ to $B_7(T)$ numerically [26]. Later, Kofke extended the study up to $B_8(T)$ [27]. Also, there are evaluations of virial coefficients for Yukawa potential and water molecules [28–30].

In the past, virial EoS has been used in many research areas in physics, ranging from thermodynamics [31–33] to nuclear physics [34] to astrophysics [35]. The renewed interest in studying the virial EoS is due to advances in theory, computing power, molecular modeling and machine-learning techniques [36]. For example, MacDowell *et al.* investigated the virial EoS for quadrupolar Lennard-Jones diatomics for a number of quadrupole moments and elongations, considering up to fourth-order virial coefficient [37]. They determined the liquid-vapor phase transition's critical temperature and pressure, which accord well with perturbation theory predictions. Mon recently used virial expansion to study the longitudinal pressure equation for hard spheres in small cylindrical pores [38]. For narrow pores, the analytical results show very good agreement for a wide range of pressures with the Monte Carlo data. Shen *et al.* calculated the virial EoS for a nonideal gas consisting of neutrons, protons, α -particles, and thousands of heavy nuclei at a subnuclear density [39].

It is well known that the evolution of the density, velocity, and granular temperature fields in the case of granular gases interacting via binary collisions is well represented by the macroscopic hydrodynamic equations for hard spherical fluids [40]. In contrast, for dense granular flows, particles remain in touch for extended periods of time, and the likelihood of three-body or more collisions is not insignificant. Finding a coarse-grained description for such dense granular flows has been an important and challenging issue in the physics of granular materials. This kind of coarse-grained representation often necessitates a link between temperature T , number density n , and pressure P . For hard-sphere interaction, such a relationship has been obtained by using virial expansion [2,41]. However, a similar study of the virial EoS for a model granular interaction that can describe dense granular flow is still missing, to the best of our knowledge.

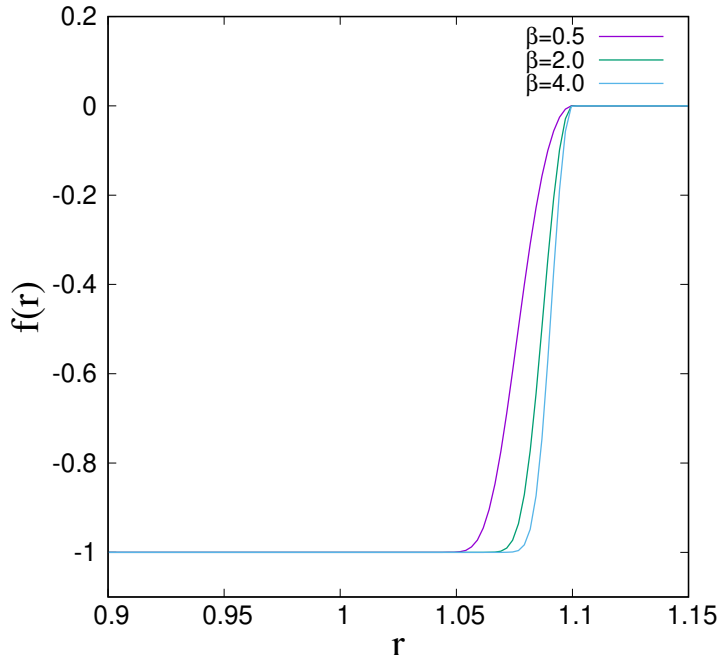


Figure 1: Plot of $f(r)$ vs. r for $\Phi(r)$ for different inverse temperature β .

In this paper, we study virial EoS for a granular potential $\Phi(r)$ as described in Sec. 2. Das *et al.* proposed this potential to study dense granular flows. Next, we integrate the expression for $B_m(T)$ s using multidimensional Monte-Carlo integration [Sec. 2.1] and importance sampling [Sec. 2.2] methods in $d = 3$. In Sec. 3, we use molecular dynamics simulation for a system of particles interacting via $\Phi(r)$ to calculate pressure (P) as a function of density n and temperature T and compare with the virial equation. Finally, we summarize our results in Sec. 4.

2. Numerical Estimation

We begin with a description of our model interaction potential. Two particles with position vectors \vec{r}_i and \vec{r}_j interact via a two-body potential of the following form:

$$\Phi(r_{ij}) = \begin{cases} \infty & ; r_{ij} < R_1, \\ V_0 \frac{(r_{ij}-R_2)^2}{(r_{ij}-R_1)^2} & ; R_1 \leq r_{ij} < R_2, \\ 0 & ; r_{ij} \geq R_2, \end{cases} \quad (6)$$

Here, $r_{ij} = |\mathbf{r}_i - \mathbf{r}_j|$ is the separation between the two particles, and V_0 is the amplitude of the potential. This potential represents a hard core of diameter R_1 surrounded by a thin repulsive interaction potential of diameter R_2 such that $R_2 - R_1 < R_1$. Eq. (6) models a repulsive potential that rises steeply from 0 at the outer boundary of the shell to infinity at the hard core, mimicking a granular interaction potential [49]. Moreover, $\Phi(r)$ reduces to the hard sphere potential in the limit $R_2 \rightarrow R_1$. In Fig. 1, we plot the Mayer function $f(r)$ as a function of pair-distance r for $\Phi(r)$ in eq. (6) for different β . Clearly, $f(r)$ is nonzero only for $r \leq R_2$.

2.1 Direct Integration Method

We calculate virial coefficients in eqs (3) – (5) by solving cluster integrals using the multi-dimensional Monte-Carlo approach in $d = 3$. Therefore, we need to solve a dm -dimensional integration to evaluate $B_m(T)$. Since the interaction potential $\Phi(r)$ is radially symmetric, we will reduce the number of integration variables by performing appropriate variable transformations. This will improve the efficiency of our numerical integrations and the convergence of our results.

To calculate $B_2(T)$, we place one particle at the origin of a spherical polar coordinate system and allow the other particle in the pair to adopt any position or orientation. The calculation for $B_2(T)$ comes down to

$$B_2 = -\frac{1}{2V} \iint f_{12} d^3r_1 d^3r_2 = -\frac{1}{2} \int f_{12}(r_{12}) d^3r_{12} = -2\pi \int_0^\infty f_{12}(r_{12}) r_{12}^2 dr_{12}, \quad (7)$$

which is a one-dimensional integral. We set the upper limit of the integral to $r_{12}^{\max} = 1.5$ because the integrand in the above equation is zero for $r_{12} > 1.1$. We obtain $B_2(T)$ by averaging over 10,000 Monte-Carlo runs. We wish to emphasize that we also calculated $B_2(T)$ by altering r_{12}^{\max} and found no significant variance.

The calculation of B_3 involves integration over three-particle clusters, as given by eq. (4). To assess such integrals, we fix a particle p1 at the origin of the spherical polar coordinate system and allow the second particle p2 to move solely along the z-axis, as illustrated in Fig. 2. We enable the third particle, p3, to take any feasible positions for a given position of p2. Finally, we repeat the procedure for different positions of p2 [42]. As a result, the eq. (4) can be expressed as

$$B_3 = -\frac{1}{3V} \iiint f_{12} f_{13} f_{23} d^3r_1 d^3r_2 d^3r_3 = -\frac{1}{3} \iint f_{12} f_{13} f_{23} d^3r_{12} d^3r_{13}. \quad (8)$$

Again, $|\mathbf{r}_{13} - \mathbf{r}_{12}| = r_{23} = \sqrt{r_{12}^2 + r_{13}^2 - 2r_{12}r_{13} \cos \phi}$, $d^3r_{13} = 2\pi r_{13}^2 dr_{13} \sin \phi d\phi$, and $d^3r_{12} = 4\pi r_{12}^2 dr_{12}$. Therefore, eq. (8) reduces to

$$B_3(T) = -\frac{8\pi^2}{3} \left[\int_0^\infty dr_{12} \int_0^\infty dr_{13} \int_0^\pi d\phi f(r_{12}) f(r_{13}) f\left(\sqrt{r_{12}^2 + r_{13}^2 - 2r_{12}r_{13} \cos \phi}\right) r_{13}^2 r_{12}^2 \sin \phi \right], \quad (9)$$

which is a three-dimensional integral. We choose $r_{12}^{\max} = r_{13}^{\max} = 2$ in our numerical simulation and obtain $B_3(T)$ by averaging over 50,000 Monte-Carlo runs.

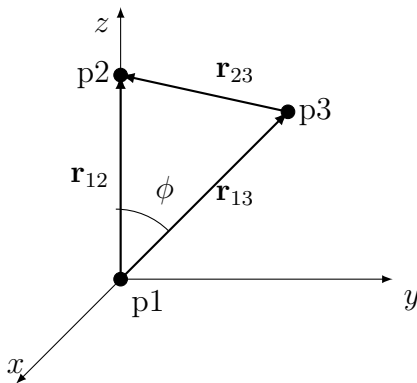


Figure 2: A schematic diagram showing the interaction among three particles.

The computation of $B_4(T)$ is linked to the assessment of four-particle cluster integrals, as provided by eq. (5). To compute $B_4(T)$, we utilize an extended version of the technique used to calculate $B_3(T)$. In this scenario, the four particles are arranged as follows: First, we fix a particle p1 at the spherical polar coordinate's origin o and constrain another particle p2 to move solely along the z -axis. Then, as illustrated in Fig. 3, we position particles p3 and p4 at i and k , respectively. As a result, the eq. (5) can be expressed in terms of r_{ij} , θ_{ij} , and ϕ . Here, r_{ij} represents the distance between the particles i and j , θ_{ij} represents the angle between the vectors \mathbf{r}_{oi} and \mathbf{r}_{oj} , and ϕ represents the angle between the oij -plane and ojk -plane. Again, $r_{ij}^2 = r_{oi}^2 + r_{oj}^2 - 2r_{oi}r_{oj} \cos \theta_{ij}$ with $i \neq j \neq o$, $\cos \theta_{ik} = \cos \theta_{ij} \cos \theta_{jk} + \sin \theta_{ij} \sin \theta_{jk} \cos \phi$ [12, 43].

$$\begin{aligned} B_4(T) &= -\frac{1}{8V} \iiint \iiint [3f_{13}f_{14}f_{23}f_{24} + 6f_{12}f_{13}f_{14}f_{23}f_{24} + f_{12}f_{13}f_{14}f_{23}f_{24}f_{34}] d^3r_1 d^3r_2 d^3r_3 d^3r_4 \\ &= -\frac{1}{8} \iiint \iiint [3f_{13}f_{14}f_{23}f_{24} + 6f_{12}f_{13}f_{14}f_{23}f_{24} + f_{12}f_{13}f_{14}f_{23}f_{24}f_{34}] d^3r_{12} d^3r_{13} d^3r_{14}. \end{aligned} \quad (10)$$

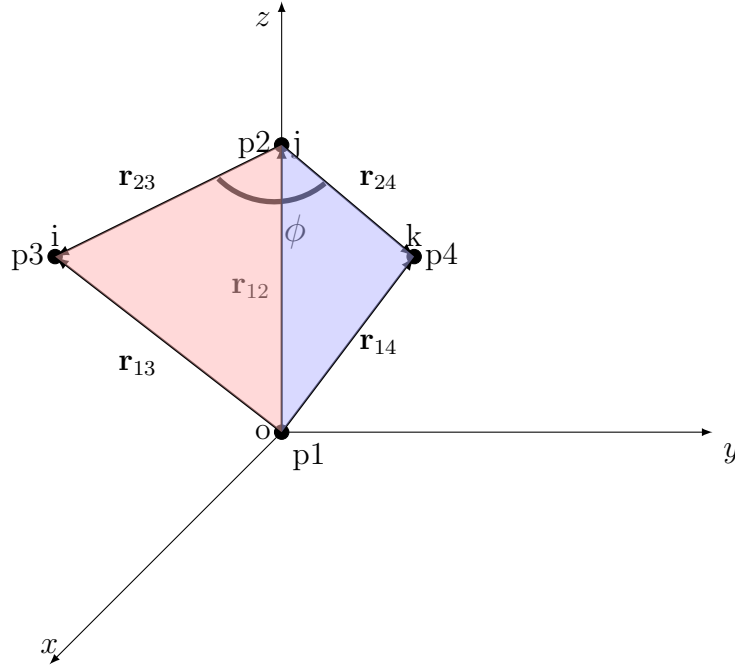


Figure 3: A schematic diagram showing a four-body cluster.

Further, the volume elements in eq. (10) reduce to $d^3r_{14} = r_{14}^2 \sin \theta_{24} dr_{14} d\theta_{24} d\phi$, $d^3r_{13} = 2\pi r_{13}^2 \sin \theta_{23} dr_{13} d\theta_{23}$, and $d^3r_{12} = 4\pi r_{12}^2 dr_{12}$. Hence, the twelve-dimensional integration in eq. (5) reduces to a six-dimensional integration in eq. (10). Now the 1st term on RHS of eq. (10) can be written as

$$\begin{aligned} D_1(T) &= -\frac{3}{8} \iiint \iiint f(r_{13})f(r_{14})f(r_{23})f(r_{24}) d^3r_{12} d^3r_{13} d^3r_{14} \\ &= -6\pi^3 \int_0^\infty \int_0^\infty \int_0^\infty \int_{-1}^1 \int_{-1}^1 r_{12}^2 f(r_{13}) r_{14}^2 f(r_{14}) r_{13}^2 f\left(\sqrt{r_{12}^2 + r_{13}^2 - 2r_{12}r_{13}\eta_{23}}\right) \\ &\quad \times f\left(\sqrt{r_{12}^2 + r_{14}^2 - 2r_{12}r_{14}\eta_{24}}\right) dr_{12} dr_{13} dr_{14} d\eta_{23} d\eta_{24}. \end{aligned} \quad (11)$$

The 2nd term on RHS of eq. (10) becomes

$$\begin{aligned}
D_2(T) &= -\frac{3}{4} \iiint f(r_{12})f(r_{13})f(r_{14})f(r_{23})f(r_{24})d^3r_{12}d^3r_{13}d^3r_{14} \\
&= -12\pi^3 \int_0^\infty \int_0^\infty \int_0^\infty \int_{-1}^1 \int_{-1}^1 r_{12}^2 f(r_{12}) r_{13}^2 f(r_{13}) r_{14}^2 f(r_{14}) f\left(\sqrt{r_{12}^2 + r_{13}^2 - 2r_{12}r_{13}\eta_{23}}\right) \\
&\quad \times f\left(\sqrt{r_{12}^2 + r_{14}^2 - 2r_{12}r_{14}\eta_{24}}\right) dr_{12}dr_{13}dr_{14}d\eta_{23}d\eta_{24}. \tag{12}
\end{aligned}$$

And the last term on RHS of eq. (10) becomes

$$\begin{aligned}
D_3(T) &= -\frac{1}{8} \iiint f(r_{12})f(r_{13})f(r_{14})f(r_{23})f(r_{24})f(r_{34})d^3r_{12}d^3r_{13}d^3r_{14} \\
&= -\pi^2 \int_0^\infty \int_0^\infty \int_0^\infty \int_{-1}^1 \int_{-1}^1 \int_0^{2\pi} r_{12}^2 f(r_{12}) r_{13}^2 f(r_{13}) r_{14}^2 f(r_{14}) f\left(\sqrt{r_{12}^2 + r_{13}^2 - 2r_{12}r_{13}\eta_{23}}\right) \\
&\quad \times f\left(\sqrt{r_{13}^2 + r_{14}^2 - 2r_{13}r_{14}\left\{\eta_{23}\eta_{24} + \sqrt{(1-\eta_{23}^2)}\sqrt{(1-\eta_{24}^2)}\cos\phi\right\}}\right) \\
&\quad \times f\left(\sqrt{r_{12}^2 + r_{14}^2 - 2r_{12}r_{14}\eta_{24}}\right) dr_{12}dr_{13}dr_{14}d\eta_{23}d\eta_{24}d\phi. \tag{13}
\end{aligned}$$

Here, we have used $\eta_{23} = \cos\theta_{23}$ [i.e., $\eta_{23} \in (-1, +1)$], $\eta_{24} = \cos\theta_{24}$ [i.e., $\eta_{24} \in (-1, +1)$], and

$$\eta_{34} = \cos\theta_{34} = \cos\theta_{23}\cos\theta_{24} + \sin\theta_{23}\sin\theta_{24}\cos\phi = \eta_{23}\eta_{24} + \sqrt{(1-\eta_{23}^2)}\sqrt{(1-\eta_{24}^2)}\cos\phi. \tag{14}$$

We obtain $B_4(T)$ by solving eqs. (11) – (13) using Monte-Carlo procedure. We use $r_{12}^{\max} = r_{13}^{\max} = r_{14}^{\max} = 2.0$ and the result is averaged over 50,000 independent runs. Table 1 shows the values of $B_2(T)$, $B_3(T)$ and $B_4(T)$ at different temperatures.

2.2 Importance Sampling Method

We calculate $B_2(T)$, $B_3(T)$, and $B_4(T)$ directly from eqs. (3) – (5) utilizing the *importance sampling* (IS) procedure [44,45]. In IS, we sample the configuration space for a m -particle cluster according to some distribution $\pi(\mathbf{r}^m; T)$ (may be unnormalized) with non-zero integrands. IS advises that we use $\pi(\mathbf{r}^m; T) = |\gamma(\mathbf{r}^m; T)|$ for better convergence of the integrations, where $\gamma(\mathbf{r}^m; T)$ is the integrand in the expression of $B_m(T)$. The *Umbrella Sampling* (US) [44] is then used to calculate a generic cluster integral $\Gamma(T)$ corresponding to the m^{th} virial coefficient. The US technique necessitates the use of a reference system for which Γ_0 (say) is the corresponding virial coefficient, after which we can write [22, 29, 46]

$$\Gamma(T) = \Gamma_0 \frac{\langle \gamma/\pi \rangle_\pi}{\langle \gamma_0/\pi \rangle_\pi}, \tag{15}$$

where $\gamma_0(\mathbf{r}^m; T)$ is the integrand in the expression of $B_m(T)$ for the reference system. For instance, if Γ is B_3 , then $\gamma = f_{12}f_{13}f_{23}$. The angular brackets represent an average over the

Table 1: $B_m(T)$ s obtained from direct integration.

T	B_2	B_3	B_4
1	2.654310	4.402244	5.359088
2	2.615108	4.272537	5.122250
3	2.589089	4.187514	4.968951
4	2.569371	4.123662	4.854866
5	2.553433	4.072416	4.763967
6	2.540037	4.029603	4.688484
7	2.528479	3.992851	4.624024
8	2.518314	3.960674	4.567848
9	2.509243	3.932078	4.518129
10	2.501057	3.906363	4.473585

configuration space $\pi(\mathbf{r}^m; T)$. Since we choose $\pi = |\gamma(\mathbf{r}^m; T)|$, then eq. (15) reduces to the following form:

$$\Gamma(T) = \Gamma_0 \frac{\langle sign \rangle_\pi}{\langle \gamma_0 / \pi \rangle_\pi}, \quad (16)$$

where *sign* can only take values +1 or -1.

Next, we select a reference system that has a high phase space overlap with the target system. As our reference system, we use the square well (SW) interaction potential, given by

$$U(r_{ij}) = \begin{cases} \infty & ; 0 < r_{ij} < R_1 \\ -\varepsilon & ; R_1 \leq r_{ij} \leq R_2, \\ 0 & ; R_2 < r_{ij}. \end{cases} \quad (17)$$

Here, R_1 is the diameter of the particles and ε is the strength of SW potential. The theoretical values of the first few virial coefficients for SW potential in $d = 3$ are [47]

$$B_2/b = 1.000 - 0.331f, \quad (18)$$

$$B_3/b^2 = 0.6250 - 0.3762f + 0.9906 \times 10^{-1}f^2 - 0.6946 \times 10^{-2}f^3, \quad (19)$$

$$B_4/b^3 = 0.2869 - 0.2207f + 0.1209f^2 - 0.4131 \times 10^{-1}f^3 + 0.6438 \times 10^{-2}f^4 \\ - 0.3090 \times 10^{-3}f^5 - 0.3023 \times 10^{-5}f^6, \quad (20)$$

where $b = 2\pi/3$ with $R_1 = 1$, $R_2 = 1.1$ and $f = \exp(\beta\varepsilon) - 1$.

To build the configuration space according to the distribution $\pi(\mathbf{r}^m; T)$, we generate a random point using a uniform random number generator in $3m$ -dimensional space. We select the

Table 2: $B_m(T)$ s using importance sampling for different ϵ .

	$\epsilon = 0.1$			$\epsilon = 0.01$			$\epsilon = 0.001$		
T	B_2	B_3	B_4	B_2	B_3	B_4	B_2	B_3	B_4
1	2.656056	4.413944	5.214216	2.655434	4.408325	5.260785	2.655377	4.407819	5.265290
2	2.617553	4.284999	5.075579	2.617144	4.282513	5.093469	2.617104	4.282263	5.095186
3	2.592008	4.193893	4.984408	2.591528	4.192988	4.997902	2.591482	4.192901	4.999225
4	2.572503	4.143922	4.899601	2.572103	4.141260	4.900358	2.572064	4.141000	4.900460
5	2.556372	4.089478	4.856408	2.556112	4.087747	4.831824	2.556086	4.087577	4.829466
6	2.543169	4.047274	4.758576	2.542882	4.045256	4.746167	2.542853	4.045058	4.744959
7	2.531828	4.017103	4.678109	2.531563	4.014324	4.663105	2.531537	4.014050	4.661648

first point (old) at the origin of the $3m$ -dimensional space. All other points (new) are generated by keeping three coordinates (coordinates of one fixed particle) at the origin and the rest of the $3(m-1)$ coordinates (rest of the $(m-1)$ particles of the cluster) by randomly perturbing between $-R_2$ and $+R_2$ with respect to the existing positions. The acceptance probability p is then calculated using the Metropolis Monte Carlo algorithm [48] as $p = \min(1, \pi^{\text{new}}/\pi^{\text{old}})$. Replace the old point with the new point if it is accepted. We continue the preceding stages until we have generated a sufficient number of points in the configuration space based on the desired distribution $\pi(\mathbf{r}^m; T)$.

Table 2 provides the numerical values of $B_2(T)$, $B_3(T)$, and $B_4(T)$ at different temperatures for three different values of ϵ obtained by importance sampling method. We notice no substantial variation in $B_i(T)$ as ϵ varies for a given T . The $B_i(T)$ values obtained from the DI and IS approaches are presented in Fig. 4. We notice that all the virial coefficients obtained by IS and DI approaches are extremely close. Further, we want to emphasize that in all the above calculations, T can be chosen freely.

Let us now discuss the advantages and disadvantages of DI and IS. In DI, we reduce the multidimensional integrations associated with the expression of virial coefficients for better convergence of numerical results. Such reduction often requires complex transformations of coordinates as we go for higher-order virial coefficients. No such reduction is required in the case of IS. In IS, we need a reference system to calculate B_i s of a target system. We choose a reference system in such a way that there is a significant overlap in the configuration spaces of both systems. In this case, the estimation of B_i s for the target system requires the value B_i for the reference system in advance, which may be approximated earlier. The DI method does not require any reference system, and thus it is free from all kind of pre-approximations. Further, we can generalize the calculation of B_i s to any arbitrary order i in the case of IS as long as we know the corresponding B_i of the reference system. No such straight-forward generalization for higher-order virial coefficients is possible for DI.

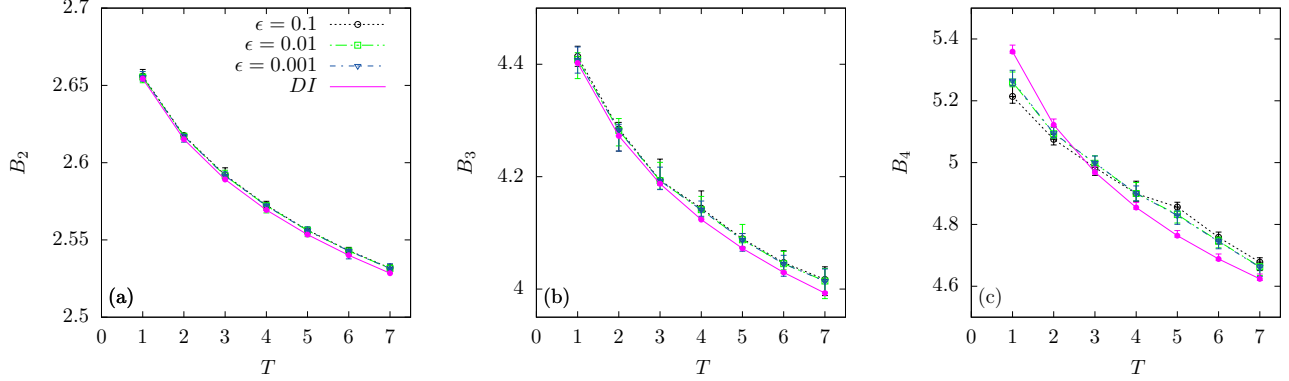


Figure 4: Plot of virial coefficients as a function of temperature T . (a) Plot of B_2 vs. T . The magenta solid line represents the result of the direct integration (DI) method. As indicated, the different line points represent data gathered using the importance sampling (IS) approach for different ϵ values. (b) Plot of B_3 vs. T , and (c) Plot of B_4 vs. T . The symbols used in (b) and (c) have the same meaning as the ones in (a).

3. Comparison with Molecular Dynamics Results

We obtain P for a system of particles interacting via $\Phi(r)$ provided by eq. (6) using molecular dynamics (MD) simulation. In this case, the normal force acting on the i^{th} particle due to the j^{th} particle is given by

$$\vec{F}_{ij}(r) = -\vec{\nabla}_j \Phi(r), \quad (21)$$

where $\vec{\nabla}_j$ is the gradient with respect to \vec{r}_j . We employ the following units for various relevant quantities: lengths are expressed in units of R_1 , energy in $u = V_0/15$, temperature in u/k_B , and time in $t_0 = \sqrt{m_0 R_1^2 / V_0}$, where m_0 is the mass of a particle. We choose $V_0 = 15$, $R_1 = 1$, and $R_2 = 1.1R_1$ since granular interactions are inherently short-ranged. We perform molecular dynamics simulations with $N = 100,000$ particles in three dimensions. We modify the linear size of the system L to achieve the desired number density, $n = N/L^3$. Given that the effective diameter of a particle is $R_2 = 1.1$, the jamming number density for our model is $n_J = 0.918$. We have carried out numerical simulations up to $n = 0.80$. In all directions, periodic boundary conditions are used. We use the velocity-Verlet algorithm to update positions and velocities with a time step of $\Delta t = 0.0005$. The temperature T of the system is given by the relation

$$\frac{3}{2}NT = \sum_{i=1}^N \frac{1}{2}m_0 \vec{v}_i^2. \quad (22)$$

In earlier work, Das *et al.* used this interaction potential to study freely evolving granular gases [49], heated granular systems in the low and high-density limits [50], and the dynamics of an intruder in granular media [51].

At $t = 0$, we randomly inject particles into the simulation box so that the cores of no two particles overlap. We assign random velocities to the particles such that the centre of mass velocity of the system is equal to zero. First, we allow the system to equilibrate until $t = 50$, which relaxes the velocity distribution to the Maxwell-Boltzmann velocity distribution. Next,

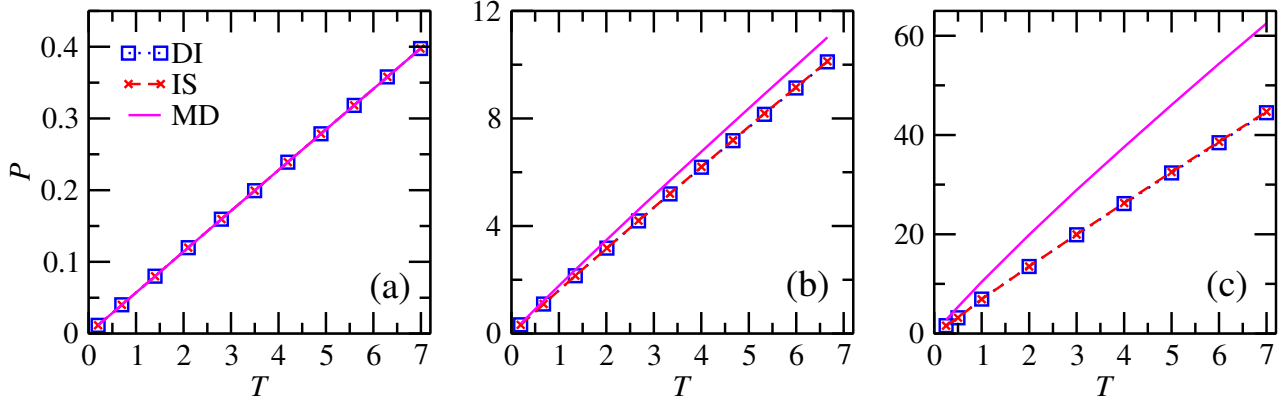


Figure 5: Pressure P vs. Temperature T plotted for different densities (a) $n = 0.05$, (b) $n = 0.45$, and (c) $n = 0.80$. The blue line-points represent a plot of eq. (1) with $B_m(T)$ s obtained from the direct integration (DI) method, the red line-points represent plot of eq. (1) with $B_m(T)$ s obtained from the important sampling (IS) method, and the solid magenta lines represent data from the molecular dynamics (MD).

we compute the elements of the stress tensor $\sigma^{\alpha\beta}$ within the volume L^3 as the sum of the contact stress and kinetic stress terms over all particles i in the system,

$$\sigma^{\alpha\beta} = \frac{1}{L^3} \sum_i \left[\sum_{j \neq i} \frac{r_{ij}^\alpha F_{ij}^\beta}{2} + m v_i^\alpha v_j^\beta \right], \quad (23)$$

where $\alpha, \beta = x, y, z$. Finally, the pressure P is given by

$$P = \frac{1}{3} [\sigma^{xx} + \sigma^{yy} + \sigma^{zz}]. \quad (24)$$

Figure 5 shows the plot of P vs. T for different densities obtained from the MD simulations and the virial EoS [eq. (1)]. Clearly, when T and n increase, so does P . The virial EoS with the first four virial coefficients is sufficient to describe the P - T graph obtained from MD simulations at low densities (cf. Fig. 5(a)). As shown in Fig. 5(b), numerical data from MD simulations are likewise in good agreement with the virial EoS with the first four virial coefficients for a intermediate $n = 0.45$ only at low- T domain. At high- T , we observe a significant deviation. For higher densities, e.g., $n = 0.80$ which is close to n_J , we see a considerable deviation at all temperatures, as illustrated in Fig. 5(c). Because many-body interactions contribute significantly to $\sigma^{\alpha\beta}$ through the contact stress, making the higher-order terms $B_m(T)n^m$ with $m \geq 5$ in virial EoS crucial.

Next, we calculate the pressure P at a fixed temperature T as a function of density n . To fix T , we rescale the velocity of all particles so that their mean kinetic energy becomes $3T/2$ and let the system equilibrate further for time $t_{\text{eq}} = 10$. Following that, we calculate T using eq. (22). This process is repeated until we reach the target T . Then we use eqs. (23) and (24) to calculate P . Figure 6 shows the plot of P vs. n for different temperatures obtained from the MD simulations and the virial EoS [eq. (1)]. Clearly, for all temperatures, the virial EoS with the first four virial coefficients is sufficient to describe the P - n graph produced from MD simulations at low densities ($n < 0.25$). For larger densities, MD data shows significant variation in all

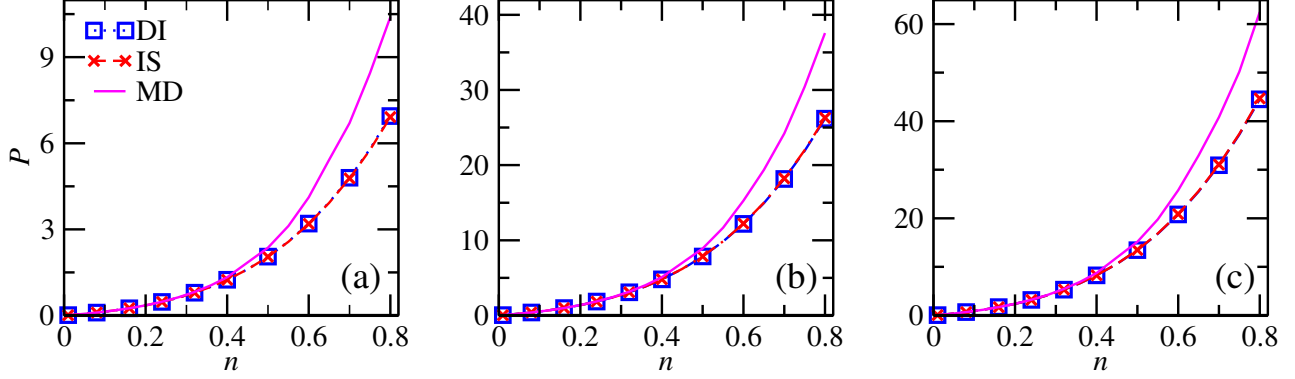


Figure 6: Plot of P vs. n for different temperatures (a) $T = 1$, (b) $T = 4$, and (c) $T = 7$. Symbols used here have the same meaning as the ones in Fig. 5.

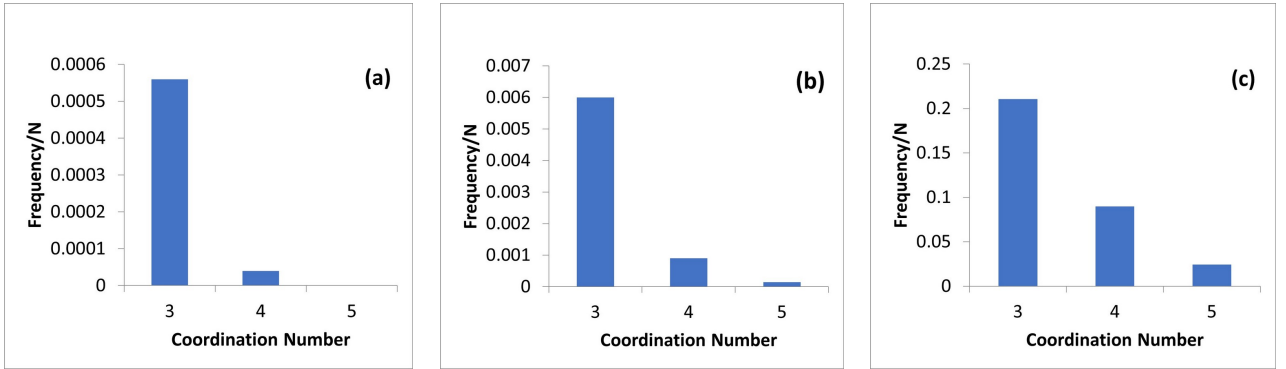


Figure 7: Plot of the distribution of coordination numbers normalized by the total number of particles N for different densities (a) $n = 0.25$, (b) $n = 0.45$, and (c) $n = 0.80$ at $T = 7$.

scenarios, highlighting the need for higher-order terms in the virial EoS. To justify our claim, we have calculated the coordination number of a particle at $T = 7$ for different densities. The distribution of coordination numbers for three densities, (a) $n = 0.25$, (b) $n = 0.45$, and (c) $n = 0.80$ is shown in Figure 7. As illustrated in Fig. 7(b), it is evident that a small fraction of particles for $n = 0.45$ have a coordination number greater than 4, which increases with increasing the density n as shown in Fig. 7(c). This indicates the necessity for $B_5(T)$ and higher-order terms in the virial EoS. However, the fraction of particles having coordination number 5 is zero for $n = 0.25$, as shown in Fig. 7(a). This holds true for all densities $n \leq 0.30$.

4. Summary and Outlook

Let us conclude this paper with a summary and discussion. We have provided a comprehensive study of the virial equation of state (EoS) for a model granular system. We calculated the first four virial coefficients for an interaction potential $\Phi(r)$ describing a granular interaction. We used two approaches: (a) direct integration and (b) importance sampling. We observed that the values of $B_2(T)$, $B_3(T)$, and $B_4(T)$ determined by these methods are extremely close.

Next, we perform a molecular dynamics simulation for a system of particles interacting via the same interaction potential. For different temperatures and densities, we calculate P using the virial stress tensor. For densities $n \leq 0.3$, the virial EoS with the first four virial coefficients is sufficiently close to the data for P obtained via MD simulations at all temperatures upto $T = 7$. MD data indicates significant deviation for dense systems, demonstrating the necessity for higher-order components in the virial EoS.

In our future endeavors, we aspire to delve deeper into the exploration of the equation of state for systems comprised of asymmetric particles. The dynamics of asymmetric particles hold a pivotal place within the realm of physics, extending their influence across various disciplines. One of the prominent arenas where the significance of asymmetric particle dynamics comes to the fore is polymer physics. Polymer chains inherently possess asymmetry, and their behavior, whether in solution or within bulk materials, is intricately linked to the intricate dynamics of individual polymer segments. Furthermore, the ramifications of asymmetric particle dynamics reverberate in the domains of soft matter and complex fluids, including gels, glasses, and liquid crystals. These materials consist of constituents that are themselves inherently asymmetric, and their behavior and properties are substantially influenced by the dynamics of these particles. The impact of this influence resonates through the field, shaping our understanding of a wide array of physical processes, materials science, and diverse technological applications.

Acknowledgments: SH acknowledges financial support from IISER Mohali through a Junior Research Fellowship. PD acknowledges financial support from SERB, India through a start-up research grant (SRG/2022/000105).

Data Availability: All of the data utilized in this manuscript will be made accessible upon reasonable request.

Author contribution statement: PD proposed the problem and develop the program for molecular dynamics simulation. SH performed the all the analytical and numerical work with the help of PD. The paper was written by PD.

References

- [1] S. J. Blundell and K. M. Blundell, *Concepts in Thermal Physics*, Oxford University Press, New York (2009).
- [2] R. K. Pathria and P. D. Beale, *Statistical Mechanics*, Academic Press, London (2021).
- [3] D. A. McQuarrie, *Statistical Mechanics*, Harper & Row, New York (1976).
- [4] S. I. Sandler, *An Introduction to Applied Statistical Thermodynamics*, John Wiley & Sons Inc, New York (2010).
- [5] B. M. McCoy, *Advanced Statistical Mechanics*, Oxford University Press Inc., New York (2010).

- [6] L. Boltzmann, Verslag. Gewone Vergadering Afd. Natuurk. Nederlandse Akad. Wtensch. **7**, 484 (1899).
- [7] M. Luban and A. Barum, J. Chem. Phys. **76**, 3233 (1982).
- [8] N. Clisby and B. M. McCoy, J. Stat. Phys. **114**, 1343 (2004).
- [9] I. Lyberg, J. Stat. Phys. **119**, 747 (2005).
- [10] T. Kihara, Rev. Mod. Phys. **25**, 831 (1953).
- [11] S. Katsura, Phys. Rev. **115**, 1417 (1959).
- [12] J. A. Barker and J. J. Monaghan, J. Chem. Phys. **36**, 2564 (1962).
- [13] F. H. Ree and W. G. Hoover, J. Chem. Phys. **40**, 939 (1964).
- [14] F. H. Ree and W. G. Hoover, J. Chem. Phys. **46**, 4181 (1967).
- [15] E J J. van Rensburg, J. Phys. A: Math. Gen. **26**, 4805 (1993).
- [16] S. Labík, J. Kolafa and A. Malijevský, Phys. Rev. E **71**, 021105 (2005).
- [17] N. Clisby and B. M. McCoy, J. Stat. Phys. **122**, 15 (2006).
- [18] H. Do, C. Feng, A. J. Schultz, D. A. Kofke and R. J. Wheatley, Phys. Rev. E **94**, 013301 (2016).
- [19] A. J. M. Garrett, J. Phys. A: Math. Gen. **13**, 379 (1980).
- [20] J. A. Barker, Proc. R. Soc. Lond. A. Mathematical and Physical Sciences **377**, 425 (1980).
- [21] J. A. Barker, P. J. Leonard and A. Pompe, J. Chem. Phys. **44**, 4206 (1966).
- [22] J. K. Singh and D. A. Kofke, Phys. Rev. Lett. **92**, 220601 (2004).
- [23] A. J. Schultz and D. A. Kofke, Mol. Phys. **107**, 2309 (2009).
- [24] C. Feng, A. J. Schultz, V. Chaudhary and D. A. Kofke, J. Chem. Phys. **143**, 044504 (2015).
- [25] M. Dixon and P. Hutchinson, Mol. Phys. **38**, 739 (1979).
- [26] R. J. Wheatley, Phys. Rev. Lett. **110**, 200601 (2013).
- [27] T. B. Tan, A. J. Schultz and D. A. Kofke, Mol. Phys. **109**, 123 (2011).
- [28] D. J. Naresh and J. K. Singh, Fluid Phase Equilib. **285**, 36 (2009).
- [29] K. M. Benjamin, A. J. Schultz and D. A. Kofke, J. Phys. Chem. C **111**, 16021 (2007).
- [30] K. M. Benjamin, J. K. Singh, A. J. Schultz and D. A. Kofke, J. Phys. Chem. B **111**, 11463 (2007).

- [31] V. G. Baonza, M. Caceres and J. Nunez, *Fluid Phase Equilibria*, **78**, 43 (1992).
- [32] L. G. MacDowell, C. Menduina, C. Vega and E. de Miguel, *Phys. Chem. Chem. Phys.*, **5**, 2851 (2003).
- [33] I. Nezbeda and W. R. Smith, *Fluid Phase Equilibria*, **216**, 183 (2004).
- [34] C.J. Horowitz and A. Schwenk, *Nuclear Physics A*, **776**, 55 (2006).
- [35] G. Shen, C. J. Horowitz and E. O’connor, *Phys. Rev. C* **83**, 065808 (2011).
- [36] A. J. Schultz and D. A. Kofke, *J. Chem. Phys.* **157**, 190901 (2022).
- [37] L. G. MacDowell, C. Menduina, C. Vega and E. de Miguel, *J. Chem. Phys.*, **119**, 11368 (2003).
- [38] K. K. Mon, *Phys. Rev. E* **97**, 052114 (2018).
- [39] G. Shen, C. J. Horowitz and S. Teige, *Phys. Rev. C* **82**, 045802 (2010).
- [40] N. V. Brilliantov and T. Poschel, *Kinetic Theory of Granular Gases* (Oxford University Press, Oxford, 2004).
- [41] N.F. Carnahan and K.E. Starling, *J. Chem. Phys.* **51**, 635 (1969).
- [42] I. M. Askerov, E. Somuncu and B. A. Mamedov, *Can. J. Phys.* **96**, 716 (2018).
- [43] B. A. Mamedov, E. Somuncu and I. M. Askerov, *AIP Conf. Proc.* **1759**, 020063 (2016).
- [44] D. Frenkel and B. Smit, *Understanding Molecular Simulation: From Algorithms to Applications 2ed*, Academic Press, London (2001).
- [45] H. Gould, J. Tobochnik and W. Christian, *An Introduction to Computer Simulation Methods 3rd ed (revised)*, San Francisco (2007).
- [46] A. J. Schultz, N. S. Barlow, V. Chaudhary and D. A. Kofke, *Mol. Phys.* **111**, 535 (2013).
- [47] E. M. Sevick and P. A. Monson, *J. Chem. Phys.* **94**, 3070 (1991).
- [48] J. S. Liu, *Monte Carlo Strategies in Scientific Computing*, Springer, New York (2004).
- [49] P. Das, S. Puri and M. Schwartz, *Phys. Rev. E* **94**, 032907 (2016).
- [50] P. Das, S. Puri and M. Schwartz, *Granular Matter* **20**, 15 (2017).
- [51] P. Das, S. Puri and M. Schwartz, *Phys. Rev. E* **102**, 042905 (2020).